Dynamics of phase separation in multicomponent mixtures

Subir K. Das and Sanjay Puri
School of Physical Sciences, Jawaharlal Nehru University, New Delhi 110067, India
(Received October 31 2001; published 24 January 2002)

We study the dynamics of phase separation in multicomponent mixtures through Monte Carlo simulations of the q-state Potts model with conserved kinetics. We use the Monte Carlo renormalization-group method to investigate the asymptotic regime. The domain growth law is found to be consistent with the Lifshitz-Slyozov law, $L(t)\sim t^{1/3}$ (where t is time), regardless of the value of q. We also present results for the scaled correlation functions and domain-size distribution functions for a range of q values.

DOI: 10.1103/PhysRevE.65.026141 PACS number(s): 64.60.−i

I. INTRODUCTION

There has been much recent interest in phase-ordering dynamics, viz., the temporal evolution of a homogeneous multicomponent mixture, which is rendered thermodynamically unstable by a sudden quench below the critical temperature [1]. After the quench, domains of different ordered phases form and grow with time as the system reaches local equilibrium on increasing length scales. For binary (AB) mixtures, where the evolving system segregates into A- and B-rich regions, the far-from-equilibrium coarsening dynamics has been studied extensively through experiments, numerical simulations, and approximate analytical methods [1]. However, the case of q-component mixtures ($q>2$) has received far less attention, though such mixtures are of obvious importance in the context of metallurgy and materials science. In this paper, we present comprehensive results from a Monte Carlo renormalization-group (MCRG) study [2,3] of segregation dynamics in the q-state Potts model with conserved kinetics, which is a simple model for phase-separating multicomponent mixtures [4].

Before we proceed, it is useful to briefly review the phenomenology for phase-ordering dynamics in binary mixtures, as this provides the context for our present study. For isotropic systems, the growth of ordered domains is characterized by a single time-dependent length scale $L(t)$ where t is the time after the quench. Therefore, the evolving morphology is invariant in time, and the order-parameter correlation function $C(r,t)$, where r is the spatial separation, exhibits a dynamical-scaling form [5]

$$C(r,t)=\langle \psi(\vec{R},t)\,\psi(\vec{r}+\vec{R},t)\rangle-\langle \psi(\vec{R},t)\rangle\langle \psi(\vec{r}+\vec{R},t)\rangle \equiv f\left(\frac{r}{L(t)}\right). \quad (1)$$

In Eq. (1), $\psi(\vec{r},t)$ is the relevant order parameter at space point $\vec{r}$ and time t; and the angular brackets refer to an averaging over initial conditions and the noise ensemble. For pure systems, the characteristic length scale exhibits a power-law behavior, $L(t)\sim t^{\phi}$, where the exponent ϕ depends upon the nature of conservation laws, relevance of hydrodynamic effects, etc. [1]. In the case with nonconserved order parameter (e.g., ordering dynamics of a ferromagnet), we have $\phi=1/2$, which is referred to as the Lifshitz-Cahn-Allen (LCA) law [6]. In the case with conserved order parameter (e.g., segregation dynamics of a binary alloy via diffusive processes), we have $\phi=1/3$, which is referred to as the Lifshitz-Slyozov (LS) law [7]. The LS growth law has been confirmed in a vast range of experiments [8] and numerical simulations [9,3].

It is important to examine the universality of these growth laws. An experimentally relevant generalization considers the dynamics of ordering in q-component mixtures. The equilibrium behavior of q-component mixtures is often understood using q-state spin models. An important example of this is the Potts model [4] with the Hamiltonian

$$H=-J\sum_{\langle ij\rangle}\delta_{S_iS_j}, \quad S_i=1,2,\ldots,q, \quad (2)$$

where $J(>0)$ is an exchange interaction that favors parallel spins. In Eq. (2), $\Sigma_{\langle ij\rangle}$ refers to a sum over nearest-neighbor pairs on the underlying lattice; and the Kronecker delta $\delta_{nm}=1$ if $n=m$ and 0 if $n\neq m$. Another important example of a q-state spin model is the clock model with the Hamiltonian

$$H=-J\sum_{\langle ij\rangle}\cos\left[\frac{2\pi}{q}(S_i-S_j)\right], \quad S_i=1,2,\ldots,q. \quad (3)$$

where the exchange interaction ($J>0$) again favors parallel spins. Clearly, Eqs. (2) and (3) are only special cases of the most general Hamiltonian for q-state spins.

The crucial difference between the Potts model and the clock model is the nature of the penalty between dissimilar spin states. In the Potts model, all pairs with $S_i\neq S_j$ are equally penalized. Thus, the equilibrium state (at nonzero temperature) consists of interfaces between domains of arbitrary spin state. There are also point defects at the junction of three types of domains—the probability of having point defects with more than three domain types is negligible, regardless of the value of q. On the other hand, in the clock model, there is a continuous variation of energy as $|S_i-S_j|$ increases. The maximum pair energy occurs for $|S_i-S_j|=[q/2]$, where $[x]$ refers to the integer part of the argument x. Therefore, the equilibrium state of the clock model (at nonzero temperature) consists of interfaces between domains of approximately similar spin states. There are also vortex-like point defects, which become equivalent to vortex defects

 ©2002 The American Physical Society

of the *XY* model in the limit $q \to \infty$. Our present study will focus upon segregation dynamics for the Potts model in Eq. (2).

This paper is organized as follows. In Sec. II, we discuss earlier results for phase-ordering dynamics in the q-state Potts model, thereby providing a background for the present study. In Sec. III, we describe our numerical techniques and the MCRG methodology. Section IV provides detailed numerical results from our simulations. Finally, Sec. V concludes this paper with a summary and discussion of the results.

II. OVERVIEW OF EARLIER RESULTS

Let us briefly examine available results for ordering dynamics in the q-state Potts model. The q-state spin models [as in Eqs. (2) or (3)] have no intrinsic dynamics. Therefore, we associate a physically appropriate stochastic dynamics with these models by placing them in contact with a heat bath. The simplest nonconserved kinetics is Glauber spin-flip kinetics, where the spin variable at a site i is ''flipped'' as $S_i \to S_i'$. Clearly, the spin composition is not conserved by this microscopic process, which is an appropriate description of ordering in q-state ferromagnets. The simplest conserved kinetics is Kawasaki spin-exchange kinetics, where the spin variables at neighboring sites (say, i and j) are interchanged as $S_i \leftrightarrow S_j$. This microscopic process conserves the spin composition of the mixture and the spin interchange mimics diffusive processes in phase-separating q-component mixtures [10]. These kinetic q-state spin models also have their coarse-grained counterparts, which consider the relaxational dynamics of $(q-1)$ order parameters with appropriate conservation laws [11].

There have been many numerical and analytical studies of the Potts model with nonconserved kinetics, and we will only discuss some representative examples here. Early Monte Carlo (MC) studies of this system in dimensionality $d=2$, 3 are due to Sahni and co-workers [12]; Kaski *et al.* [13]; and Kumar *et al.* [14]. A comprehensive MCRG study of the $q=8$ Potts model on a two-dimensional (2D) triangular lattice was subsequently performed by Roland and Grant [15]. An alternative approach is due to Lau *et al.* [16], who undertook a 2D Langevin simulation of the corresponding field-theoretic model [17]. These numerical studies demonstrate that the domain-growth law is consistent with the LCA law, $L(t) \sim t^{1/2}$, for all values of q. Furthermore, the above numerical studies also found that the scaled correlation function (or its Fourier transform, the scaled structure factor) for the q-state Potts model were comparable to that for the $q=2$ (Ising) case.

It is appropriate to clarify the various regimes for domain growth in the Potts model. The characteristic angle between neighboring spins on the lattice is $\theta(t) \sim 1/L(t)$, as the domain size measures the typical interdefect spacing. At early times, $\theta(t)$ is larger than the quantization angle $\theta_q = 2\pi/q_d$, where $q_d=3$ for three-domain point defects. (The Potts and clock models are equivalent for $q=3$ [4]—therefore, the three-domain point defects of the Potts model are equivalent to the vortex-like point defects of the three-state clock model.) Thus, at early times, the local spin variable is effectively continuous and the system behaves similar to the dynamical *XY* model [18,19]. The discrete spin structure is seen when $\theta(t) \simeq \theta_q$, or $L(t) \simeq L_c \sim \text{const} \times q_d$. This corresponds to the crossover from *XY*-like behavior to Ising-like behavior [20]. However, there is no crossover in the growth law because the LCA law characterizes coarsening resulting from annihilation of both interfacial and vortex defects [18,19].

A more recent analytical and numerical study of the nonconserved Potts model is due to Sire and Majumdar (SM) [21], who argued that the evolution of the q-state Potts model is equivalent to the evolution of an Ising system with magnetization $m = \langle S_i \rangle = 2/q - 1$. SM demonstrated that the domain-growth law is $L(t) \sim t^{1/2}$ for arbitrary q values. They also obtained approximate analytical results for the real-space correlation function using Mazenko's Gaussian closure scheme [22,1].

There have been far fewer studies of the Potts model with conserved kinetics, and the physical situation is not as clear as in the nonconserved case. An early MC study in $d=2$ is due to Grest and Sahni (GS) [23], who reported a very low growth exponent $\phi \simeq 0.2$ for the cases with $q=3$, 6. This result was refuted by Jeppesen and Mouritsen (JM) [24], who performed a 2D MC study of the conserved three-state Potts model under critical quench conditions, i.e., all components were present in equal proportions. JM found that the GS study had underestimated the growth exponent due to long-lived transients, and the asymptotic growth law was consistent with the LS law, $L(t) \sim t^{1/3}$. The numerical results of JM have been confirmed in an exchange MC study by Okabe [25]. Recently, Tafa *et al.* [26] have undertaken 2D MC simulations of phase separation in ternary mixtures, and categorized evolution morphologies and growth laws in different regions of the parameter space. The three-state Potts model is a special case of their general study, which reports an asymptotic LS growth law for a wide range of evolution morphologies.

To the best of our knowledge, there has been no systematic study of the q-state Potts model ($q>3$) with conserved kinetics. The asymptotic growth regime should be consistent with the LS growth law, as the dominant growth mechanism is the annealing of domain boundaries. However, there are transient effects that give rise to slower growth laws and interfere with the observation of the asymptotic regime. Firstly, as we have argued before, the early-time behavior is governed by the annihilation of vortexlike defects. In contrast to the nonconserved case, there is a distinct growth law associated with vortex annihilation in the conserved *XY* model, i.e., $L(t) \sim t^{1/4}$ in $d=2$ and $L(t) \sim (t \ln t)^{1/4}$ in $d=3$ [1,27,28]. The crossover from vortex-driven growth to interface-driven growth occurs when $L(t) \simeq L_c$. The dependence of $L(t)$ on q can be determined by the following simple argument. In the homogeneous state prior to the quench, the density of a spin species $\sim q^{-1}$, where we consider the case of a critical quench. If the domain formation time is t_0, the initial domain scale is $L_0 \sim q^{-1/d} (D t_0)^{1/2}$, where D is the spin diffusion constant. (We assume that the initial domain formation occurs by random spin motion.)

Thus, the prefactor in the domain-growth law scales with q as $q^{-1/d}$ and the crossover time scale is $t_c \sim q^{4/d} q_d^4$. Because of the extreme discreteness of the point defects ($q_d = 3$), this crossover occurs rather early in our simulations. For a more accurate estimate of crossover time scales and prefactors, we should also account for the q dependence of the surface tension, which depends upon $|T_c - T|$ and the appropriate critical exponent [4]. We will discuss this point in greater detail later.

Another important transient effect is the diffusion of spins along interfaces, rather than through the domain bulk, which also yields the slower growth law, $L(t) \sim t^{1/4}$ [29,30]. This effect is enhanced at higher temperatures, where the domain boundaries are rough, and for higher q values, where the domain length scales are smaller at a given time. The asymptotic growth regime is accessed when the interfacial thickness σ (which is constant in time) becomes irrelevant compared to the diverging domain length scale $L(t)$ [31,32], i.e., $\sigma/L(t) \to 0$. We will subsequently describe and use a MCRG procedure to facilitate the observation of the late-stage behavior.

III. NUMERICAL TECHNIQUES AND THE MONTE CARLO RENORMALIZATION GROUP

The Potts model is defined by the Hamiltonian in Eq. (2). We performed 2D MC simulations of the Potts model with Kawasaki spin-exchange kinetics on a square lattice. At time $t = 0$, the system was quenched from $T = \infty$ to $T < T_c$, where $T_c [= J/\ln(1+\sqrt{q})]$ is the critical temperature for $d = 2$ [4]. (The Boltzmann constant k_B is set to unity.) The system size was N^2 and periodic boundary conditions were imposed in both directions. The initial condition for each run consisted of a random mixture of all spin states in equal proportion, mimicking the high-temperature state before the quench. The microscopic kinetics preserves the numbers of each spin state. The far-from-equilibrium homogeneous system evolves according to the standard MC procedure: a pair of randomly selected nearest-neighbor spins (S_i and S_j) is interchanged with probability p, where

$$p = 1 \qquad \text{if } \Delta E \leqslant 0,$$

$$= \exp\left(-\frac{\Delta E}{T}\right) \quad \text{if } \Delta E > 0. \tag{4}$$

In Eq. (4), ΔE is the change in energy due to the spin exchange,

$$\Delta E = J \sum_{k \in L_i, k \neq j} (\delta_{S_i S_k} - \delta_{S_j S_k}) + J \sum_{k \in L_j, k \neq i} (\delta_{S_j S_k} - \delta_{S_i S_k}), \tag{5}$$

where L_i refers to the nearest neighbors of i.

The unit of time is 1 Monte Carlo step (MCS), which corresponds to N^2 attempts to update spins on the lattice. The results presented here correspond to the case of random MC updates. We have confirmed that the results are unchanged if we use a sequential updating procedure also. Our simulations were performed for $q = 2$, 3, 4, 5, 6, 8, 10, 12 at $T = 0.85 T_c$. The case $q = 2$ corresponds to the Ising model and will serve as a reference point for the results presented here. We will subsequently present results for evolution morphologies, real-space correlation functions, domain-size distribution functions, and domain-growth laws. All statistical results presented here are obtained for lattice sizes $N = 512$ (prior to renormalization), and as averages over ten independent runs.

We analyze the evolution of the system using the MCRG technique, which was originally developed in the context of equilibrium statistical physics by Ma [2], and was subsequently extended by Swendsen and others [33]. The first application of the MCRG method to nonequilibrium problems was a study of critical dynamics by Tobochnik *et al.* [34]. Subsequently, Vinals and others used this approach to investigate ordering dynamics in Ising models [35] and q-state Potts models [36] with nonconserved kinetics. In this paper, we follow the formulation of Roland and Grant [3], who have used this method to study spinodal decomposition in the $d = 2$ Ising model with conserved kinetics.

Before we proceed, it is relevant to briefly describe the MCRG approach in the present context. In the asymptotic growth regime, the system is scale invariant, provided that space and time are rescaled by the appropriate factors. The relationship between the rescaling factors for space and time is determined by the domain-growth law. Consider a ''block-spin'' transformation on the evolving system at time t, where we map a block of b^d spins $\{S_i\}$ (where b is the scale factor) into a single spin S_i'. A simple implementation of the blocking procedure is a majority rule, where the entire block is assigned the value S_i', corresponding to the majority state in the block. For blocks with equal numbers of two (or more) states n and m, we randomly assign the value n or m to the block spin. The RG procedure leads to a slight violation of the conservation law, but we have confirmed numerically that the error is negligible [3,37]. In the scaling regime, the length scales of the renormalized patterns at the mth and $(m+1)$th levels of this simple RG procedure are related to each other as

$$L(m,t) = L(m+1, b^{1/\phi} t), \tag{6}$$

where ϕ is the growth exponent.

We should stress that Eq. (6) is independent of the RG procedure, and also applies for lattices that have been merely rescaled by a factor $1/b$ without any associated ''block-spin'' transformation. The major advantage of the RG procedure is that it eliminates nonuniversal features on short length scales and enables investigation of asymptotic properties. As we mentioned earlier, there are two important length scales in phase-ordering systems: (a) the time-dependent domain length $L(t)$ and (b) the time-independent interface thickness σ, which is equivalent to the correlation length ξ. The asymptotic regime is accessed when $\sigma/L(t) \to 0$ [31]. Near the critical point, σ (and ξ) are large and this considerably delays the onset of the asymptotic regime. The simple RG procedure described above reduces interfacial fluctuations, and thereby the effective interfacial thickness. In this sense, the RG procedure drives the evolving system towards the

zero-temperature fixed point. The general arguments presented here will be further clarified by our numerical results, presented in Sec. IV.

IV. NUMERICAL RESULTS

In this section, we present detailed numerical results obtained from the simulations described above. The renormalization scale factor is chosen to be $b=2$, i.e., a block of four spins is mapped onto a single spin at each level of renormalization.

A. Evolution morphologies

Figure 1 shows the evolution pictures resulting from a random initial condition for the cases $q=3$, 4, 5, and 10. The panels on the left show evolution patterns at $t=10^6$ MCS without renormalization (corresponding to $m=0$, where m refers to the level of renormalization). For clarity, we use the following coding procedure for each snapshot. The domain boundaries are marked as solid lines, and minority spins in bulk domains are marked as crosses. At the relatively high simulation temperatures we use, there are a considerable number of ''impurity'' spins in bulk domains. Furthermore, notice that the evolution patterns are primarily comprised of interfaces and point defects, which are three-domain junctions. As we have argued earlier, we expect the temporal evolution to be governed by the annihilation of interfaces. The panels on the right show the corresponding evolution patterns at the $m=1$ level of renormalization. The RG procedure strongly suppresses fluctuations, as is evident from a comparison of panels on the left and right. The noise reduction is a crucial feature of the MCRG procedure and enables us to access the asymptotic behavior of the evolving system.

The reduction of fluctuations could also be achieved by reducing the system temperature. However, this results in the evolving system becoming trapped in metastable states, particularly for large values of q. The presence of these metastable states makes it difficult to access the asymptotic regime in low-temperature simulations.

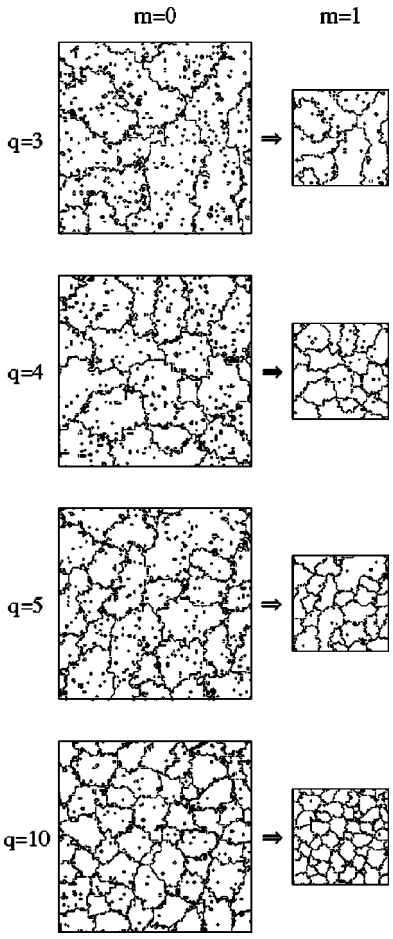

FIG. 1. Evolution pictures at $T<T_c$ for the q-state Potts model with Kawasaki spin-exchange (conserved) kinetics. Our 2D MC simulations were performed on N^2 lattices with periodic boundary conditions in both directions. The initial condition for each run consisted of a random mixture of equal amounts of the q different spin states. The temperature for each run is $T=0.85T_c$, where $T_c=J/\ln(1+\sqrt{q})$ for the q-state Potts model [4]. (The Boltzmann constant k_B is set to unity.) The unrenormalized system size was $N=256$. The panels on the left show snapshots (128^2 corner of the 256^2 system) for $q=3$, 4, 5, 10 at time $t=10^6$ MCS after the quench. Each snapshot shows the domain boundaries (marked as solid lines) and the impurity spins in bulk domains (marked as crosses). The panels on the right show renormalized patterns (64^2 corner of the 128^2 system) at the $m=1$ level, obtained through the ''block-spin'' mapping described in the text.

B. Real-space correlation functions

The numerical data for the real-space correlation function, and other statistical quantities presented here, was obtained at the $m=3$ level of renormalization. The correlation function for the Potts model is computed as follows [15]. A given Potts state (say, n) is designated as $+1$, and all other states are designated as -1. Thus, at a certain site i, we define the Ising variable $\sigma_i^n=2\delta_{S_{i,n}}-1$. The equal-time correlation function is then defined as

$$C(r,t)=\frac{1}{q}\sum_{n=1}^{q}\left[\langle\sigma_i^n(t)\sigma_j^n(t)\rangle-\langle\sigma_i^n(t)\rangle\langle\sigma_j^n(t)\rangle\right], \quad (7)$$

where r is the distance between points i and j. The angular brackets in Eq. (7) refer to an averaging over independent initial conditions and the noise ensemble. As the composition of the mixture is fixed, we expect $\langle\sigma_i^n(t)\rangle=\langle\sigma_j^n(t)\rangle=2/q-1$, though our RG procedure slightly violates this equality.

Figure 2 shows the scaled correlation functions for the evolution depicted in Fig. 1. Figure 2(a) plots $C(r,t)/C(0,t)$ versus $r/L_c(t)$ for the case $q=4$ from three different times. The scaling length $L_c(t)$ is defined as the point where the correlation function decays to half its maximum value. The reasonable data collapse demonstrates that the evolving system exhibits dynamical scaling. Figure 2(b) plots $C(r,t)/C(0,t)$ versus $r/L_c(t)$ at $t=2.5\times10^6$ MCS for different values of q, i.e., $q=2$, 3, 4, 5, 10. The scaled correlation function clearly depends upon the q value for the conserved

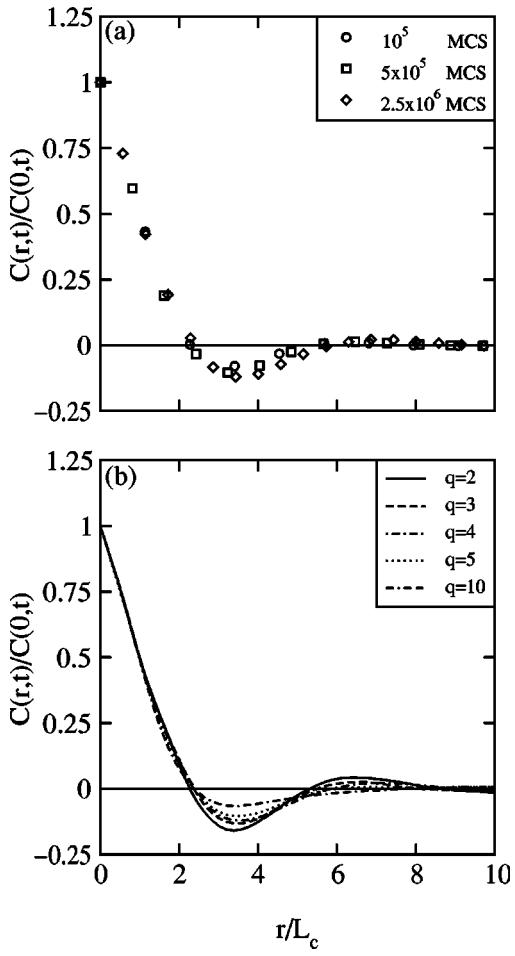

FIG. 2. (a) Scaling plot of the real-space correlation function $C(r,t)$ for the case $q=4$. The data corresponds to $m=3$ renormalized patterns, obtained from systems of original size $N=512$. We superpose data for $C(r,t)/C(0,t)$ versus r/L_c from three different times, denoted by the indicated symbols. The characteristic length scale $L_c(t)$ is defined as the r value where the correlation function decays to half its maximum value. (b) Comparison of scaled correlation functions for $q=2$, 3, 4, 5, 10—denoted by the specified line types. The data sets correspond to $m=3$ renormalized patterns at $t=2.5\times10^6$ MCS.

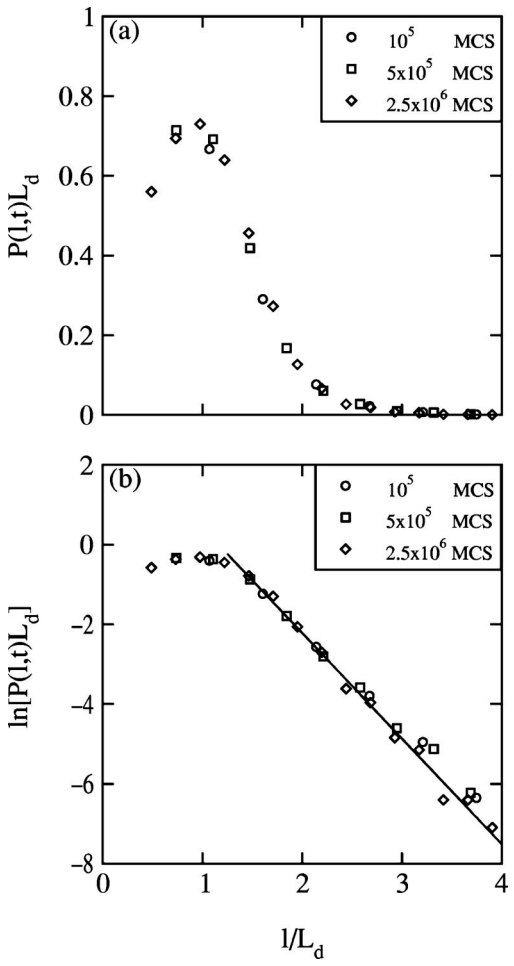

FIG. 3. (a) Scaling plot of the domain-size probability distribution function $P(l,t)$ for the case $q=4$. The definition of $P(l,t)$ is provided in the text. As in Fig. 2, the data corresponds to $m=3$ renormalized patterns, obtained from systems of original size $N=512$. We superpose data for $P(l,t)L_d$ versus l/L_d (where $L_d=\langle l\rangle$) from three different times, as indicated. (b) Semilog plot of the data in (a). The solid line is a linear fit to the tail region.

Potts model, as our definition of the correlation function is equivalent to that for an Ising model with off-critical composition $\langle\sigma_i\rangle=2/q-1$. In the context of the Ising model with conserved kinetics, it is well known that the correlation function varies continuously with the degree of off-criticality [9].

C. Domain-size distribution functions

Figure 3 plots the domain-size distribution functions for the evolution depicted in Fig. 1. Again, all numerical data corresponds to the $m=3$ level of renormalization. The domain-size distribution $P(l,t)$, where l is the domain size, is obtained by examining domain boundaries along horizontal and vertical cross sections of evolution snapshots, as shown in Fig. 1. The distribution function is normalized as $\int_0^\infty dl P(l,t)=1$. The scaling form of the domain-size distribution function is $P(l,t)=L_d(t)^{-1}g(l/L_d(t))$, where $L_d(t)$ is a measure of the characteristic domain size, e.g., $L_d(t)=\langle l\rangle$. Figure 3(a) is a plot of $P(l,t)L_d$ versus l/L_d for $q=4$ from three different times and confirms the scaling of the domain distribution function. Figure 3(b) is a semilog plot of the data in Fig. 3(a) and exhibits a characteristic exponential decay for the scaling function [26].

Figure 4 demonstrates that the scaled probability distribution also varies continuously with q. Figure 4(a) plots $P(l,t)L_d(t)$ versus $l/L_d(t)$ for $q=2$, 3, 4, 5, 10 at $t=2.5\times10^6$, and the scaling functions are seen to differ systematically in the tail region. Figure 4(b) is a semilog plot of the data in Fig. 4(a), and clarifies the difference in the tail region of the scaling functions—the decay is faster for larger values of q. The evolution pictures in Fig. 1 provide a qualitative reason for this difference—domains for higher q values are more compact and the probability of deviation from the average length scale is less. For lower q values, merger events between domains of similar spin states give rise to large fluctuations about the average length scale.

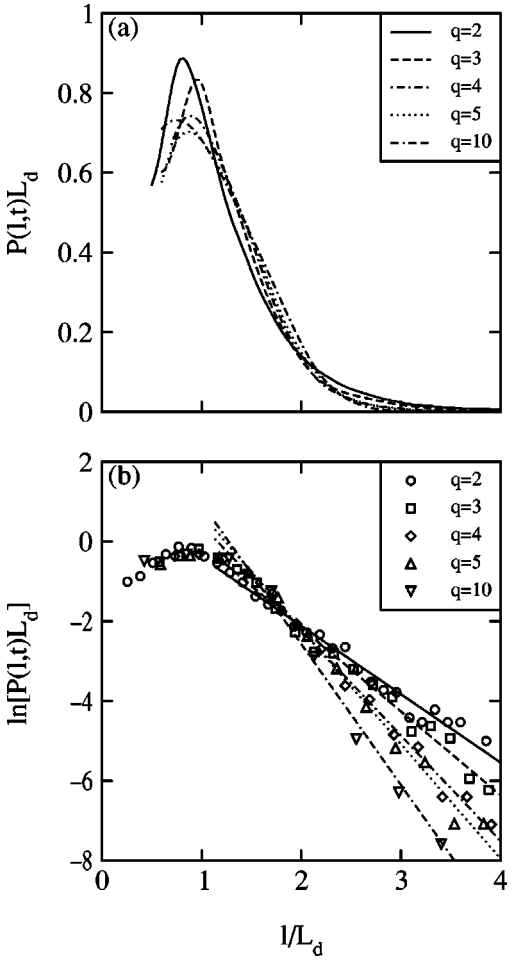

FIG. 4. (a) Comparison of the scaled domain-size distributions for the cases $q=2$, 3, 4, 5, 10, denoted by the specified line types. The data sets correspond to $m=3$ renormalized patterns at $t=2.5\times10^6$ MCS. (b) Semilog plot of the data in (a), plotted using indicated symbols. For clarity, we also show the best linear fits to the tail region.

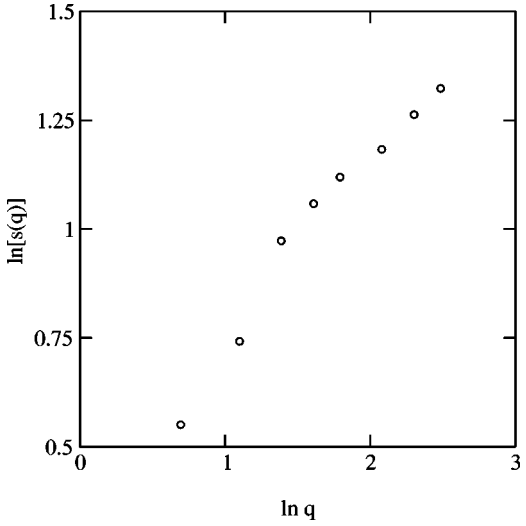

FIG. 5. Plot of $\ln[s(q)]$ versus $\ln q$, where $-s(q)$ is the slope of the tail region for the scaled probability distributions in Fig. 4(b). Notice that we have also included data for $q=6$, 8, 12, which were not shown in Fig. 4. A linear fit to the data for $q>3$ yields a slope $\simeq 0.31\pm0.01$.

The compactness of the evolution morphology can be quantified through the dependence of the decay slope in Fig. 4(b) [designated as $-s(q)$] on q. Figure 5 plots $\ln[s(q)]$ versus $\ln q$ for the various q values shown in Fig. 4(b), in conjunction with data for $q=6$, 8, 12. For $q\to\infty$, we expect $s(q)\to\infty$, as the distribution function becomes very sharply peaked about the average size. The data points for $q>3$ in Fig. 5 can be reasonably fitted to a power law with exponent $=0.31\pm0.01$. However, in the absence of a reliable analytical argument, our numerical data is inadequate to specify an unambiguous functional form for $s(q)$.

D. Domain-growth laws and exponents

Finally, let us examine the relevant domain-growth laws. In the scaling regime, all measures of the characteristic length scale are equivalent upto prefactors. We use the most direct measure of the length scale, i.e., $L_d(t)=\langle l\rangle$, the first moment of the domain-size distribution function. Figure 6(a) plots $L_d(t)$ versus t for $q=3$. We show results for $m=0$ (without renormalization) and $m=3$ (at the third level of renormalization). The data for $m=0$ is seen to be considerably noisy. If we fit the $m=0$ data to the nonlinear form $L(t)=a+bt^{\phi}$, the resultant growth exponent is $\phi\simeq0.20$. This is much less than the asymptotic exponent of $\phi=1/3$, expected on the basis of the curvature-reduction mechanism [6]. On the other hand, the data for $m=3$ is seen to be far smoother (even though it is obtained for effectively smaller lattice sizes) and the best-fit exponent is $\phi=0.30$, which is consistent with the LS growth law. The corresponding nonlinear fits are denoted as solid lines on the appropriate data sets. We should stress that the length scales for $m=0$ patterns are only a factor $\simeq 3$ larger than the length scales for $m=3$ patterns, even though the RG scale factor is $2^3=8$. This is because the extreme noisiness of the $m=0$ patterns ''breaks'' up bulk domains, leading to a substantial underestimation of length scales obtained from the probability distribution function. On the other hand, the length scale for $m=2$ patterns (not shown here) is approximately two times the length scale for $m=3$ patterns, which is consistent with the RG scale factor.

Figure 6(b) is analogous to Fig. 6(a) but for the case $q=4$. The relevant best-fit exponents are specified in the figure. Figures 6(c) and 6(d) correspond to the cases with $q=5$ and 10, respectively, but only show the $m=3$ data. In all these cases, the growth exponent is seen to be consistent with the LS law. We emphasize that the unambiguous observation of this result is facilitated by our MCRG procedure. The unrenormalized data consistently underestimates the growth exponent on the time scales of our simulation, regardless of the measure of length scale.

Figures 6(a)–6(d) are plotted on the same scale so as to facilitate a comparison of time scales of growth for different q values. Recall that the initial domain size $L_0\sim q^{-1/2}$ for $d=2$, and this provides the q dependence of the prefactor for the time-dependent length scale. Figure 7 plots

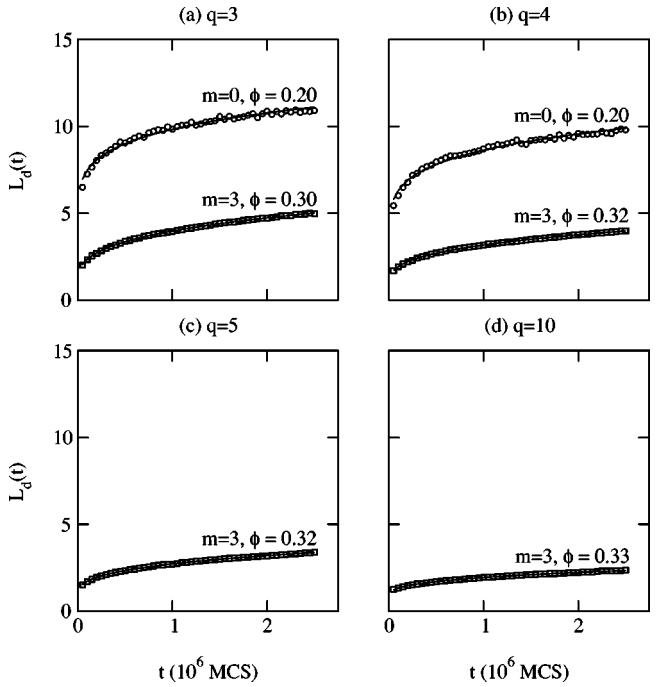

FIG. 6. Time dependence of the characteristic domain size $L_d(t)$, obtained as the first moment of the probability distribution $P(l,t)$. The solid lines superposed on the various data sets are nonlinear fits to the form $L(t)=a+bt^{\phi}$. The corresponding value of the best-fit exponent is specified in the figure. The error bars on the exponent estimates are ± 0.01. (a) Data for $q=3$ from the bare ($m=0$) patterns and the renormalized ($m=3$) patterns. (b) Data for $q=4$ from the $m=0$ and $m=3$ patterns. (c) Data for $q=5$ from the $m=3$ patterns. (d) Data for $q=10$ from the $m=3$ patterns.

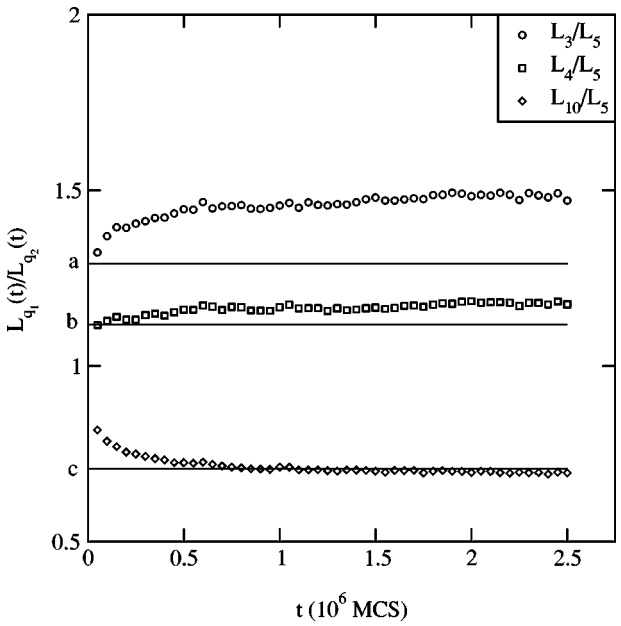

FIG. 7. Plot of $L_{q1}(t)/L_{q2}(t)$, where $L_q(t)$ is the length scale for the q-state Potts model, obtained from $m=3$ patterns. We present data for $q_1=3$, 4, 10 and $q_2=5$—denoted by the indicated symbols. The horizontal lines are drawn at $a=\sqrt{5/3}$, $b=\sqrt{5/4}$, and $c=\sqrt{5/10}$.

$L_{q1}(t)/L_{q2}(t)$ versus t for the cases $q_1=3$, 4, 10 and $q_2=5$. For $q_1=4$ and 10, the length-scale ratio is consistent with the expected value of $\sqrt{q_2/q_1}$. A possible source of the discrepancy for $q_1=3$ is the weak q dependence of the surface tension. Recall that we had $T=0.85T_c$ in our simulations and the surface tension $\sigma_{\rm st}\sim|T_c-T|^{\nu(q)}\sim[\ln(1+\sqrt{q})]^{-\nu(q)}$, where $\nu(q)(>0)$ is the relevant critical exponent [4]. In our RG procedure, it is difficult to estimate the renormalized value of the surface tension, though for $T=0$, we have $\sigma_{\rm st}=J$, regardless of the q value.

We can also estimate the growth exponent by comparing data at different levels of renormalization as in Eq. (6). We compare domain-growth data for $m=2$ and $m=3$ and ascertain times t (for $m=2$) and t' (for $m=3$), where the length scales are equal. The corresponding growth exponent is then estimated as

$$\phi_{\rm eff}(t)=\frac{\ln b}{\ln(t'/t)}$$

$$\equiv\frac{\ln 2}{\ln(t'/t)}. \qquad (8)$$

Figure 8 plots $\phi_{\rm eff}(t)$ versus $1/L_d(t)$ for $q=3$, 4, 5, 10 (as in Fig. 6), where $L_d(t)$ refers to the length scale for $m=3$ patterns. Huse [29] has studied the approach of the growth ex-

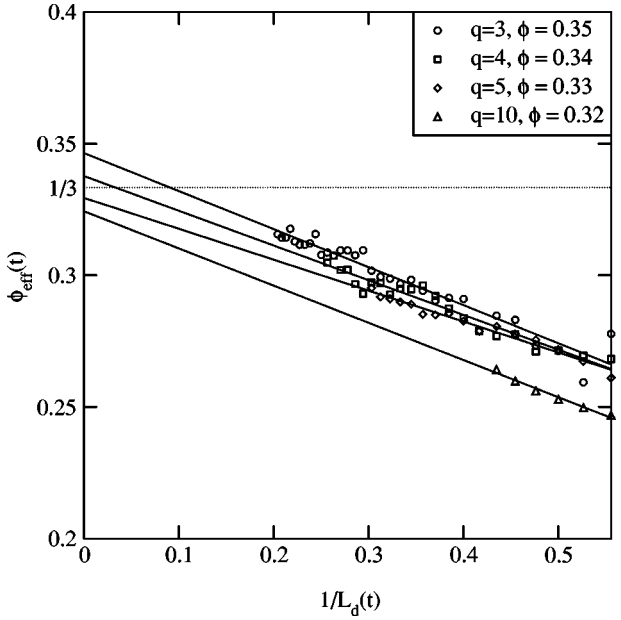

FIG. 8. Plot of effective exponent $\phi_{\rm eff}(t)$ versus $1/L_d(t)$, where $L_d(t)$ refers to the length scale obtained from renormalized ($m=3$) patterns. The effective exponent is obtained by comparing length scales at $m=2$ and $m=3$ levels of renormalization, as explained in the text. We present data for $q=3$, 4, 5, 10. The best linear fits to the data are denoted by solid lines, and are extrapolated to $L_d(t)=\infty$, yielding an estimate of the asymptotic exponent. The exponent estimates for different q values are specified in the figure.

ponent $\phi \to 1/3$ (the LS value) for spinodal decomposition in the Ising model. He determines the finite-time corrections to the LS exponent as

$$\phi_{\rm eff}(t) = \frac{1}{3} - \frac{\alpha}{L(t)} + \frac{\beta}{L(t)^2} + \cdots , \tag{9}$$

where α, β, etc. are constants. In Fig. 8, we attempt linear fits to our data, as suggested by the first two terms on the right-hand side of Eq. (9). The extrapolation of these linear fits to $L_d(t) = \infty$ (or $t = \infty$) provides an estimate for the asymptotic growth exponent. The appropriate values are specified in the figure, and are again consistent with the LS growth law.

V. SUMMARY AND DISCUSSION

Let us conclude this paper with a summary and discussion of the results presented here. We have undertaken a comprehensive Monte Carlo renormalization-group (MCRG) study of phase-separation dynamics in multicomponent mixtures, modeled by the q-state Potts model with conserved kinetics. Domain growth in this model is driven by the evaporation-condensation mechanism, which enables the annealing of interfacial defects or domain boundaries. Thus, we expect domain growth to be in the Ising universality class, consistent with the Lifshitz-Slyozov (LS) growth law, $L(t) \sim t^{1/3}$. Our simulations unambiguously demonstrate this for a range of q values. We stress that the elimination of fluctuations by the MCRG procedure is a critical element for the observation of the correct asymptotic behavior. We could also suppress fluctuations by reducing the system temperature, but then the evolving system becomes trapped in metastable states—this effect is more pronounced at higher q values. Thus, the MCRG procedure utilized here appears to be the only viable means of accessing the asymptotic regime for the conserved Potts model with reasonable computing effort.

We have also presented results for the scaling forms of the correlation functions and domain-size distribution functions. The scaled correlation function for the q-state Potts model varies with q, and is equivalent to that for phase separation in the Ising model with off-criticality $\langle \sigma_i \rangle = 2/q - 1$. The scaled domain-size distribution also varies with q. In particular, the exponentially decaying tail falls off more rapidly for larger values of q, as the more compact domain morphology suppresses large fluctuations in the domain size. In the absence of reliable analytical arguments, it is difficult to quantify the q dependence of the slope.

Our present study had two major goals. First, we have again demonstrated the utility of the MCRG procedure in accessing the asymptotic regime for evolving nonequilibrium systems. Second, we have provided an anthology of detailed numerical results for the asymptotic regime of domain growth in multicomponent mixtures. These results should be of considerable relevance to subsequent experimental and analytical studies of this problem.

ACKNOWLEDGMENT

S.K.D. is grateful to the University Grants Commission, India for financial support.

[1] For reviews, see J. D. Gunton, M. San Miguel, and P. S. Sahni, in *Phase Transitions and Critical Phenomena*, edited by C. Domb and J. L. Lebowitz (Academic Press, New York, 1983), Vol. 8, p. 267; K. Binder, in *Phase Transformations of Materials*, edited by R. W. Cahn, P. Haasen and E. J. Kramer, Materials Science and Technology Vol. 5 (VCH, Weinheim, 1991), p. 405; A. J. Bray, Adv. Phys. **43**, 357 (1994).

[2] S. K. Ma, Phys. Rev. Lett. **37**, 461 (1976).

[3] C. Roland and M. Grant, Phys. Rev. Lett. **60**, 2657 (1988); Phys. Rev. B **39**, 11 971 (1989).

[4] For a review of equilibrium properties and applications of the Potts model, see F. Y. Wu, Rev. Mod. Phys. **54**, 235 (1982), and references therein.

[5] K. Binder and D. Stauffer, Phys. Rev. Lett. **33**, 1006 (1974); Z. Phys. B **24**, 406 (1976).

[6] I. M. Lifshitz, Sov. Phys. JETP **15**, 939 (1962); S. M. Allen and J. W. Cahn, Acta Metall. **27**, 1085 (1979).

[7] I. M. Lifshitz and V. V. Slyozov, J. Phys. Chem. Solids **19**, 35 (1961).

[8] For example, see B. D. Gaulin, S. Spooner, and Y. Morii, Phys. Rev. Lett. **59**, 668 (1987).

[9] For example see Y. Oono and S. Puri, Phys. Rev. Lett. **58**, 836 (1987); Phys. Rev. A **38**, 434 (1988); S. Puri and Y. Oono, *ibid.* **38**, 1542 (1988).

[10] K. Kawasaki, in *Phase Transitions and Critical Phenomena*, edited by C. Domb and M. S. Green (Academic Press, New York, 1972), Vol. 2, p. 443.

[11] P. C. Hohenberg and B. I. Halperin, Rev. Mod. Phys. **49**, 435 (1977).

[12] P. S. Sahni, G. S. Grest, M. P. Anderson, and D. J. Srolovitz, Phys. Rev. Lett. **50**, 263 (1983); P. S. Sahni, D. J. Srolovitz, G. S. Grest, M. P. Anderson, and S. A. Safran, Phys. Rev. B **28**, 2705 (1983); G. S. Grest, D. J. Srolovitz, and M. P. Anderson, *ibid.* **38**, 4752 (1988).

[13] K. Kaski, J. Nieminen, and J. D. Gunton, Phys. Rev. B **31**, 2998 (1985).

[14] S. Kumar, J. D. Gunton, and K. Kaski, Phys. Rev. B **35**, 8517 (1987).

[15] C. Roland and M. Grant, Phys. Rev. B **41**, 4663 (1990).

[16] M.-H. Lau, C. Dasgupta, and O. T. Valls, Phys. Rev. B **38**, 9024 (1988).

[17] R. K. P. Zia and D. J. Wallace, J. Phys. A **8**, 1495 (1975).

[18] A. J. Bray and S. Puri, Phys. Rev. Lett. **67**, 2670 (1991); H. Toyoki, Phys. Rev. B **45**, 1965 (1992).

[19] A. J. Bray and A. D. Rutenberg, Phys. Rev. E **49**, R27 (1994); A. D. Rutenberg and A. J. Bray, *ibid.* **51**, 5499 (1995).

[20] S. Puri, R. Ahluwalia, and A. J. Bray, Phys. Rev. E **55**, 2345 (1997).

[21] C. Sire and S. Majumdar, Phys. Rev. Lett. **74**, 4321 (1995); Phys. Rev. E **52**, 244 (1995).

[22] G. F. Mazenko, Phys. Rev. B **42**, 4487 (1990).
[23] G. S. Grest and P. S. Sahni, Phys. Rev. B **30**, 226 (1984).
[24] C. Jeppesen and O. G. Mouritsen, Phys. Rev. B **47**, 14 724 (1993).
[25] Y. Okabe, New J. Phys. **1**, 10.1 (1999).
[26] K. Tafa, S. Puri, and D. Kumar, Phys. Rev. E **64**, 056139 (2001); **63**, 046115 (2001).
[27] M. Mondello and N. Goldenfeld, Phys. Rev. E **47**, 2384 (1993); M. Siegert and M. Rao, Phys. Rev. Lett. **70**, 1956 (1993).
[28] S. Puri, A. J. Bray, and F. Rojas, Phys. Rev. E **52**, 4699 (1995); F. Rojas, S. Puri, and A. J. Bray, J. Phys. A **34**, 3985 (2001).
[29] D. A. Huse, Phys. Rev. B **34**, 7845 (1986).
[30] S. Puri, A. J. Bray, and J. L. Lebowitz, Phys. Rev. E **56**, 758 (1997).
[31] Y. Oono and S. Puri, Mod. Phys. Lett. B **2**, 861 (1988).
[32] S. Puri and Y. Oono, J. Phys. A **21**, L755 (1988).
[33] For a review, see R. H. Swendsen, in *Real-Space Renormalization*, edited by T. W. Burkhardt and J. M. J. van Leeuwen (Springer-Verlag, New York, 1982), p. 57, and references therein.
[34] J. Tobochnik, S. Sarker, and R. Cordery, Phys. Rev. Lett. **46**, 1417 (1981).
[35] J. Vinals, M. Grant, M. San Miguel, J. D. Gunton, and E. T. Gawlinski, Phys. Rev. Lett. **54**, 1264 (1985).
[36] J. Vinals and J. D. Gunton, Phys. Rev. B **33**, 7795 (1986).
[37] M. C. Yalabik and J. D. Gunton, Phys. Rev. B **25**, 534 (1982).